Nuclear Engineering and Design, 355 (2019) 110321, https://doi.org/10.1016/j.nucengdes.2019.110321

Post-test simulation of a PLOFA transient test in the CIRCE-HERO facility

V. Narcisi*, F. Giannetti*, A. Del Nevo°, M. Tarantino°, G. Caruso*

* DIAEE – Nuclear Section, "Sapienza" University of Rome, Rome, Italy

° ENEA FSN-ING, Brasimone R.C., Camugnano (Bo), 40033, Italy

Abstract

CIRCE is a lead-bismuth eutectic alloy (LBE) pool facility aimed to simulate the primary system of a heavy liquid metal (HLM) cooled pool-type fast reactor. The experimental facility was implemented with a new test section, called HERO (Heavy liquid mEtal pRessurized water cOoled tubes), which consists of a steam generator composed of seven double-wall bayonet tubes (DWBT) with an active length of six meters. The experimental campaign aims to investigate HERO behavior, which is representative of the tubes that will compose ALFRED SG. In the framework of the Horizon 2020 SESAME project, a transient test was selected for the realization of a validation benchmark. The test consists of a protected loss of flow accident (PLOFA) simulating the shutdown of primary pumps, the reactor scram and the activation of the DHR system.

A RELAP5-3D© nodalization scheme was developed in the pre-test phase at DIAEE of "Sapienza" University of Rome, providing useful information to the experimentalists. The model consisted to a mono-dimensional scheme of the primary flow path and the SG secondary side, and a multi-dimensional component simulating the large LBE pool. The analysis of experimental data, provided by ENEA, has suggested to improve the thermal-hydraulic model with a more detailed nodalization scheme of the secondary loop, looking to reproduce the asymmetries observed on the DWBTs operation. The paper summarizes the post-test activity performed in the frame of the H2020 SESAME project as a contribution of the benchmark activity, highlighting a global agreement between simulations and experiment for all the primary circuit physical quantities monitored. Then, the attention is focused on the secondary system operation, where uncertainties related to the boundary conditions affect the computational results.

1. Introduction

The Horizon 2020 SESAME project (thermal-hydraulics Simulation and Experiment for the Safety Assessment of Metal cooled reactor) supported the development of innovative liquid metal-cooled reactor technologies by developing and validating advanced numerical approaches for their design and safety assessment. For this purpose, the project promoted the realization of experimental campaigns focused on the improvement of knowledge and on the extension of validation data base. In this framework, a validation benchmark was proposed to investigate capabilities of different computational codes to predict the main thermal-hydraulic phenomena in a heavy liquid metal-cooled pool-type fast reactor. Four participants were involved in the benchmark exercise: ENEA, SCK-CEN and "Sapienza" University of Rome used different versions of RELAP5, and NRG used a coupled approach adopting the system thermal-hydraulic code SPECTRA and the commercial code ANSYS CFX (SESAME Project, EURATOM H2020, 2015). In this paper, the post-test calculations performed by "Sapienza" University of Rome within the validation benchmark promoted in H2020 SESAME project, are presented.

The validation benchmark concerns the experimental campaign performed in the lead-bismuth eutectic alloy (LBE) integral test facility CIRCE (CIRColazione Eutettico), equipped with a new test section, called HERO (Heavy liquid mEtal pRessurized water cOoled tubes), consisting in a double wall bayonet tubes (DWBT) steam generator (SG). The main purposes of the experimental campaign were to prove feasibility and performance of a DWBT SG in a relevant configuration for ALFRED SG (Frignani et al., 2017), and to provide experimental data suitable for code validation (Lorusso et al., 2019a).

Code assessment plays a key role in the application for safety analysis and licensing of the innovative reactors. The thermal-hydraulic system codes (TH-SYS) are qualified for a wide variety of accident scenarios involving the light-water cooled reactors (LWR), but the growing interest in the innovative coolants, such as heavy liquid metals (HLM), make essential to validate the improved versions of the codes, which include models and correlations concerning these fluids.

In addition, the pool-type reactor was presented as one of the most promising configurations for the so-called Generation IV (GEN IV) reactors (OECD Nuclear Energy Agency, 2017), reducing the likelihood of loss of coolant accidents due to elimination of piping external to the primary vessel and maintaining significant thermal inertia. The presence of a large amount of quasi-stagnant liquid metal within the primary vessel introduces critical points for the reactor modelling, related to the thermal hydraulics of the pool. In literature, three approaches were found for the simulation of liquid metal pool-type systems, using Computational Fluid Dynamics (CFD) codes (Edemetti et al., 2019), TH-SYS codes (Narcisi et al., 2019b in this issue), or a combination of the two (Angelucci et al., 2017).

Part of the H2020 SESAME project was focused on thermal hydraulic analysis of liquid metal pool. In this framework, the use of CFD as computational code for the design, control, and analysis of HLM-cooled pool-type reactors was investigated. Two different CFD models of CIRCE facility were developed, showing a good agreement with experimental data even if some discrepancies are found in the pool stratification (Zwijsen et al., 2019 in this issue).

Application of CFD for long lasting transient simulations could be limited due to the computational costs. In this regard, several examples of standalone TH-SYS codes application for liquid metal pool modelling were found in literature. The most used approach is to divide large pool into multiple channels, adopting cross junctions to reproduce buoyancy. This methodology was applied for the post-test simulations of CIRCE-ICE experimental campaign. ENEA and “Sapienza” University of Rome (UNIROMA1) developed two different models assessing the capabilities of two versions of RELAP5: ENEA used a modified version of RELAP5/MOD3.3 (Bandini et al., 2015) and UNIROMA1 used RELAP5-3D, which is the latest version in the series of RELAP (Narcisi et al., 2019a). The simulations highlighted good capabilities of the codes to reproduce the main thermal-hydraulic aspects, even if some discrepancies were found in the prediction of the pool thermal stratification. Another approach is to model the pool with a multi-dimensional (MULTID) component, developed and introduced in RELAP5-3D to allow the user to model more accurately the three-dimensional hydrodynamics (The RELAP5-3D© Code Development Team, 2015a). The assessment of the MULTID capabilities was presented in Narcisi et al. (2019a), where the multi-dimensional modelling approach was compared with the multiple channel methodology. The comparison with experimental data highlighted an improved resolution adopting the MULTID component. In quasi-stagnant liquid metal pool, thermal conduction could assume a relevant role in the thermal stratification. This aspect was investigated in CIRCE-ICE post-test analysis, implementing a dedicated thermal conduction model within the pool. The results were comparable with the previous calculations (without thermal conduction model) and the negligible improvements did not justify the much higher computational costs (Narcisi et al., 2019a).

The CIRCE-HERO nodalization scheme, developed for the pre-test calculations (Narcisi et al., 2018), was improved starting from the information obtained during the blind phase of the benchmark exercise. The MULTID modelling approach was adopted for the LBE pool and a detailed mono-dimensional nodalization scheme was developed for the primary flow path and for the secondary loop. Computational results are compared with experimental data, focusing on the analysis of relevant phenomena occurring in the experimental test:

- the transition from gas-enhanced circulation (GEC) to natural circulation (NC);
- the heat transfer within the fuel pin simulator (FPS);
- the steam generator (SG) heat transfer;
- the heat losses;
- the pressure drops;
- the pool thermal stratification.

2. CIRCE-HERO test facility

2.1. Description of the test facility

CIRCE is a multipurpose facility aimed to investigate the main features of HLM-cooled pool-type reactors. It is composed of the main vessel, filled with about 70 tons of molten LBE and designed to host different test sections, and two auxiliary tanks for the maintenance phase and the liquid metal drainage (Turroni et al., 2001). The test section (TS) was refurbished with a steam generator consisting in a bundle of seven DWBTs (Figure 1). Figure 2 depicts a schematic view of HERO TS, highlighting the primary flow path. Cold LBE enters the unit through the feeding conduit, connected to the lower plenum of the facility. The feeding conduit is equipped with a Venturi flow meter (FM) to measure the mass flow rate passing through the 800 kW fuel pin simulator. The heat source (HS) consists of 37 electrically heated pins, with an active length of 1 m, arranged in a hexagonal bundle characterized by a pitch to diameter ratio (p/d) equal to 1.8 (Tarantino et al., 2015). The rods are kept in the correct position with a lower grid, that allows the LBE inlet, 3 spacer grids, located at the inlet, middle and outlet sections of the active zone (red in Figure 2), and an upper grid, that forces the coolant to move inside the fitting volume. The hot LBE moves upward along the riser, consisting in a double wall pipe, insulted with air gap. At the inlet section of the riser, argon is injected within the test section to enhance the coolant circulation; the argon injection line descends inside the pool, it passes through the lower plate of the fitting volume, and the gas is injected through a nozzle installed at the riser inlet. The mixture is collected into the separator, which achieves the separation of the two phases: argon flows upward towards the gas-plenum and LBE moves downward inside the SG. In addition, the separator works as an expansion volume, to absorb the oscillations of the LBE free level during the transients. The steam generator consists in a bundle of seven DWBTs, arranged in a hexagonal lattice, characterized by a p/d of 1.42. Five spacer grids limit the vibration of the bayonet tubes, ensuring their correct position within the hexagonal shell. Thermal insulation between the component and the pool is obtained adopting a double wall shell with air gap. Figure 3 provides a view of the relative positions of the main components included inside the primary vessel. The dead volume is located above the FPS, allowing the passage of the HS rods. The power dissipated along the cold pin tails is removed with air flow rate; in order to reduce the heat exchanged between this component and the cold pool, the dead volume is included within a double wall insulated pipe.

The steam generator is characterized by an active length of 6 m. Primary coolant flows downward through the free volume between the DWBTs and the hexagonal shell, and then it is released into the main pool. Figure 1 shows a schematic view of the DWBT, consisting in four concentric tubes. Feedwater (FW) enters the unit at the top edge of the inner tube, moving downward up to the lower plenum, where flow is inverted. Then, secondary

coolant moves upward in the annular riser between second and third tube, where the boiling occurs. The steam, exiting the seven DWBTs, is collected inside the steam chamber and then it is released to the steam discharge line. The volume between inner and second tube is filled with an insulator, to prevent the steam condensation on the outside wall of the second tube; the gap between third and fourth tube is filled with pressurized helium and high thermal conductivity powder. The helium pressure is monitored to detect any possible leakages and the heat exchange performance is guaranteed by the high conductivity powder. Secondary loop is completed with the feeding line, equipped with a demineralizer, a volumetric piston pump, a helical pre-heating system, a manifold, which distributes the feedwater to the seven bayonet tubes, and a bypass line used for the start-up phases (Lorusso et al., 2018).

The whole facility is equipped with a detailed monitoring system. An overall number of 170 thermocouples (TC) is installed to acquire temperature along primary and secondary systems (Lorusso et al., 2019a). The FPS is equipped with 39 TCs which measure LBE temperature in different subchannels and wall temperature of three pins in different axial positions of the active length. An overall number of 42 TCs are installed in primary and secondary side of the SG, acquiring temperature in several positions. One of the main tasks of the experimental campaign is to investigate relevant three-dimensional phenomena within the LBE pool; for this purpose, 119 TCs are installed inside the pool in 9 azimuthal positions (the support rods are identified from A to I in Figure 3) and several axial levels that cover the whole height of the facility. The acquisition of LBE temperature is intensified in two sectors: at the level of the fitting volume, where large heat losses occur, and at the top level of the HS active length, where a thermal stratification phenomenon was expected (Narcisi et al., 2018).

Pressure on both primary and secondary systems is acquired with 10 bubble tube purge pressure transducers and the total feedwater flow rate is measured with a Coriolis FM downstream the secondary pump; in addition, six of the seven DWBTs are equipped with a turbine flow meter at the inlet edges, monitoring the secondary flow rate passing through each bayonet element (Lorusso et al., 2019a).

2.2. Experimental test

The experimental transient test, selected for the code assessment, consists of a protected loss of flow accident (PLOFA), simulating the loss of primary pump, the reactor scram and the activation of the decay heat removal (DHR) system. Test starts at full power conditions, with 356 kW supplied to the HS and 2.75 Nl/s of argon injected to promote primary circulation. Some uncertainties are related to measurement of the feedwater mass flow rate through the secondary loop. As reported in Lorusso et al. (2019a), assuming a water density of 640 kg/m^3 and considering uniform distribution of the flow rate among the seven DWBTs, a total mass flow rate of 0.26 kg/s is obtained. This assumption is not confirmed by the experimental data; tube 1, that is not equipped with the turbine FM, is fed by higher mass flow rate, as demonstrated by the temperature acquired at the DWBTs outlet section. At the outlet of tubes 0, 3 and 4 superheated conditions are observed, whereas, at tube 1 outlet, saturated conditions are measured (TCs installed at the outlet section of tubes 2, 5 and 6 loss the signal during the test). The lack of information about steam quality at the outlet of tube 1, does not allow the estimation of the flow rate but a higher value is expected. In addition, the measured flow rate through tubes 0, 3, 4 and 5 highlights discrepancies in the magnitude of 10 %. In Lorusso et al. (2019a) an estimation of the FW mass flow rate is obtained from energy balance equation applied to the pre-heater, but this value is affected by uncertainty of the system efficiency. For these reasons, the Coriolis measurement is assumed as boundary condition for the full power calculation. This flow meter is installed downstream the volumetric piston pump and its measurements are affected by large fluctuations, probably induced by the pump (an accumulator is installed between pump and flow meter to reduce these fluctuations), which represent a large source of uncertainty. For the simulation, the mean value of 0.34 kg/s measured by the Coriolis FM is considered. FW is pre-heated to the inlet temperature of 609 K and the pressure of steam discharge line is regulated to 172 bar (Lorusso et al., 2019a).

The transition of FPS power, FW inlet conditions and Ar injection occurs at the same time. The HS thermal power decreases to 5% of the nominal value in 240 s, following a characteristic HLM-cooled reactor decay heat curve; the Ar injection decreases to zero in 124 s, simulating the presence of a pump flywheel and the FW mass flow rate is reduced to 30% of the nominal flow reproducing the activation of a DHR system, maintaining the same inlet temperature and outlet pressure on the secondary loop (Lorusso et al., 2019a).

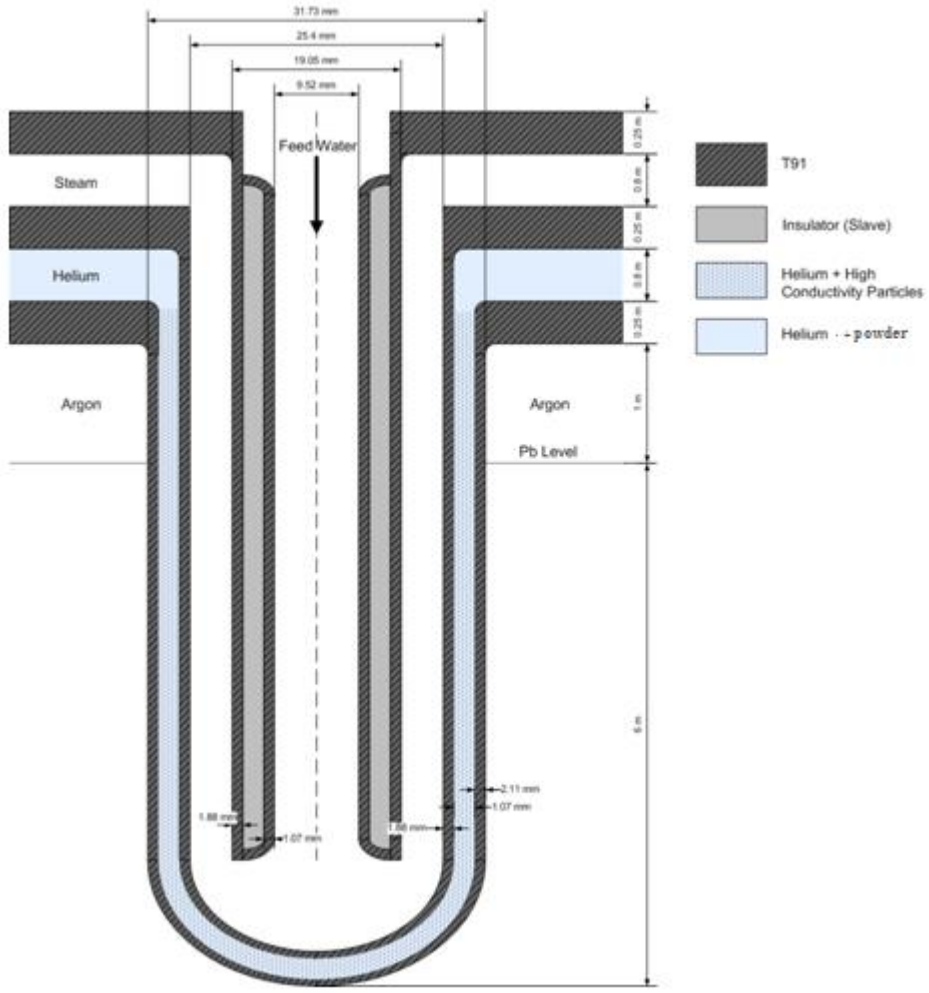

Figure 1. Double wall bayonet tube

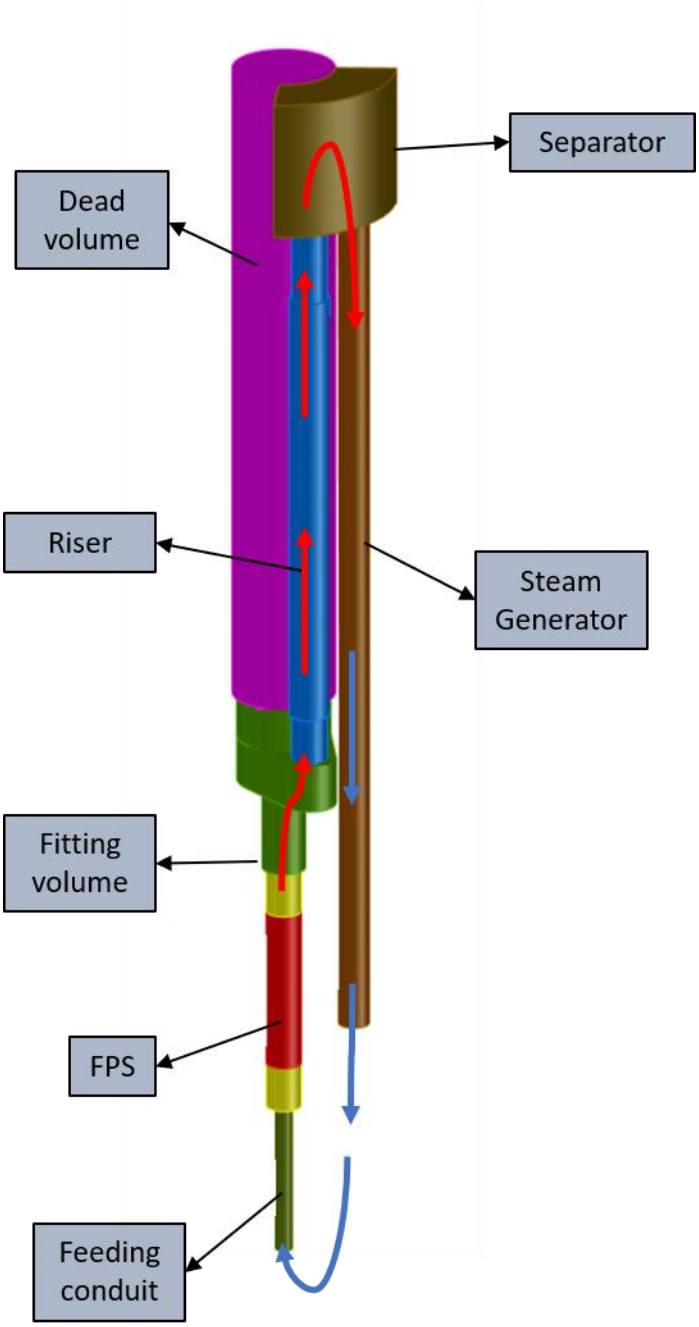

Figure 2. HERO test section

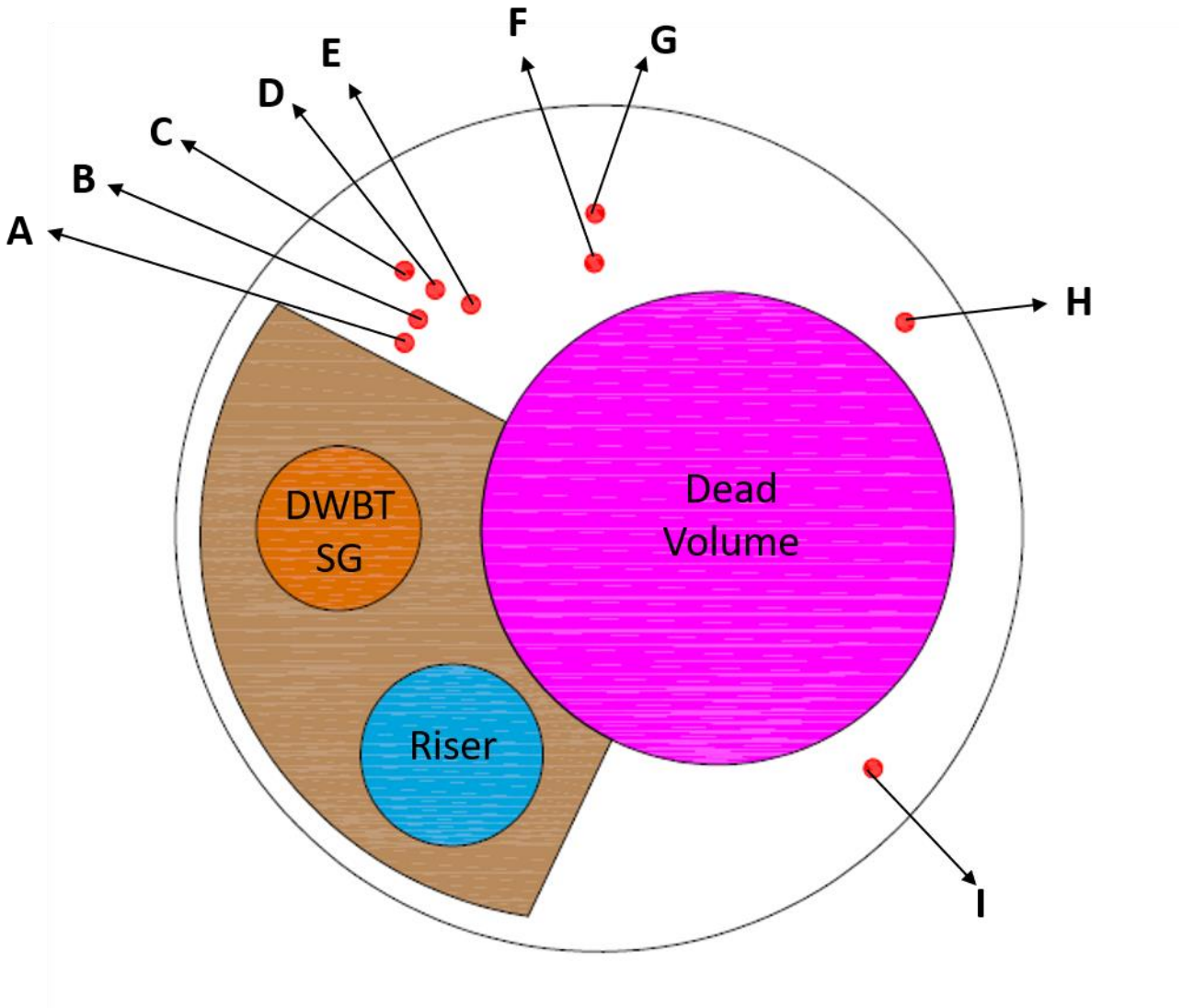

Figure 3. Instrumentation rods within the pool

3. CIRCE-HERO thermal hydraulic model

RELAP5-3D© (R5-3D) is the latest version of RELAP series. Developed at Idaho National Laboratory (INL), RELAP5-3D is a generic thermal-hydraulic system code that can be used in large range of nuclear and non-nuclear system analysis. Previous versions of RELAP5 were developed and widely validated for safety analysis and licensing of the LWR. In last years, the growing interest in the innovative reactors encourages developers to introduce new features that allow three-dimensional analysis of large volumes, such as pools, and simulation of engineering systems which imply the employment of new working fluids, such as HLM or molten salt. These innovative features are fully integrated in RELAP5-3D and they need to be validated (The RELAP5-3D© Code Development Team, 2015a).

The nodalization scheme, used for pre-test simulations and for blind calculations, was developed starting from the validated thermal-hydraulic model of CIRCE-ICE, that represents the previous configuration of the facility (Narcisi et al., 2017a). The geometrical scheme was revamped for simulation of the new test section, including a

relative coarse nodalization of the steam generator, consisting of a single equivalent double wall bayonet tube with a weight of seven (Narcisi et al., 2017b). The comparison between blind calculations and experimental data showed some discrepancies, attributable to an overestimation of the power removed by the SG (Lorusso et al., 2019b). The differences could be in large part explained by the not uniform feedwater distribution through the seven DWBTs. In addition, after the transition event, the thermocouple installed at the inlet section of tube 6 measured a superheated temperature that could be explained by a blockage occurring along this tube. These considerations suggested to improve the thermal-hydraulic model, including a detailed nodalization of the secondary loop. Furthermore, the model used for blind simulations predicted reverse flow condition through the hot leg of the primary system in the first minutes after the transition event, that is not acquired by the instrumentation (Lorusso et al., 2019b). The analysis performed during the post-test phase highlighted the relationship between reverse flow and pressure drops through the primary system: the whole pressure drops were well predicted by the code, as confirmed by the steady state LBE mass flow rate, but the distribution of the pressure losses through the flow path seemed to be wrong. In particular, the model over predicted the pressure drop through the SG and, when LBE flow rate assumed low values, the mass flow through the SG was stopped and a reverse flow condition was observed on the hot leg. In order to reduce this effect, the thermal-hydraulic model has been enhanced with an improved distribution of the pressure losses through the primary flow path.

The model consists of two macro-regions: a mono-dimensional scheme of primary and secondary systems, and a multi-dimensional model of the pool. Figure 4 shows the mono-dimensional nodalization scheme of primary and secondary systems. Feeding conduit (in green) is the lowest component of the test facility, representing the inlet section. It is modelled as an insulated pipe component, assuming that heat losses towards the pool are negligible. The Venturi flow meter is considered with a local K-loss coefficient, dependent on the flow conditions (Narcisi et al., 2017a):

$$K_{Venturi} = 10.5\, Re^{-0.016}$$

where the Reynolds number is evaluated within the feeding conduit.

Cold LBE enters the fuel pin simulator passing the lower grid; the pressure drop related to lower and spacer grids are calculated with Rehme correlation, depending on the flow conditions (Schikorr et al., 2010):

$$\Delta p_{grid} = C_v \cdot \varepsilon^2 \cdot 0.5 \cdot \rho \cdot v^2$$

where ρ and v represent the LBE density and velocity and ε is the blockage factor, calculated as the ratio between the area occupied by the grid and the free flow area. The parameter C_v is evaluated as:

$$C_v = MIN\left[3.5 + \frac{73.14}{Re^{0.264}} + \frac{2.79 \cdot 10^{10}}{Re^{279}}, \frac{2.6}{\varepsilon^2}\right]$$

The FPS is simulated with subchannel modelling approach, adopting 72 mono-dimensional parallel pipes (from 801 to 872 in Figure 4). Figure 5 shows the subchannel nodalization scheme, highlighting three different channel types, depending on the position within the bundle: 54 inner subchannels, 6 edge subchannels and 12 corner subchannels. Each pipe component is axially divided in 16 control volumes, identifying the three relevant axial zones of the HS: 3 volumes for the bottom mixing zone (see Figure 4, in yellow), 8 for the active length (in red) and 5 for the top mixing zone (in yellow). The axial division allows the comparison of the temperature calculated in the exact position of the TCs installed within the HS. Flow area and equivalent hydraulic diameter are evaluated per each subchannel type, according to the geometry presented in Figure 5. As described in Memmott et al. (2010), the correct evaluation of cross flow represents a crucial aspect on the use of RELAP5 as a subchannel code. For this purpose, 1536 cross junctions are implemented in the model, connecting each control volume of

adjacent subchannels. Cross flow depends on the pressure gradient and on the hydraulic resistance. In order to obtain a good evaluation of the cross flow, junction area is calculated as the lateral flow area between two adjacent rods, considering the length of each control volume, and the hydraulic resistance is evaluated as a K-loss coefficient depending on the flow condition. Idelchik (1986) provides a correlation for the evaluation of the K-loss coefficient for cross flow in bundle of staggered pins:

$$K = \left(z_p + 1\right) \cdot A \cdot \varphi \cdot Re^{-0.27}$$

where the parameter *A* is calculated as:

$$A = 3.2 + 0.66a_1$$

$$a_1 = (1.7 - \bar{s})^{1.5}$$

For CIRCE-HERO FPS geometry, φ and $\bar{s}$ are equal to 1. According with this correlation, the K-loss coefficient implemented per each cross junction is:

$$K = 7.17 \cdot Re^{-0.27}$$

Thermal power supplied by the electrical heated rods is simulated with 5760 heat transfer active nodes, providing a fraction of the total power proportional to the heat transfer area characterizing each control volume and considering a flat power distribution into the bundle (according with experiment). For the evaluation of the heat transfer coefficient (HTC) in bundle geometry for liquid metals, R5-3D uses Westinghouse correlation (The RELAP5-3D© Code Development Team, 2015b):

$$Nu = 4.0 + 0.33\left(\frac{p}{d}\right)^{3.8}\left(\frac{Pe}{100}\right)^{0.86} + 0.16\left(\frac{p}{d}\right)^{5}$$

developed in the ranges of 1.1<p/d<1.4 and 10<Pe<5000. CIRCE-HERO FPS bundle is characterized by a p/d equal to 1.8, out of the Westinghouse validity range. As presented in Giannetti et al. (2016) a good estimation of the HTC is obtained with Ushakov correlation (Ushakov et al., 1977):

$$Nu = 7.55\frac{p}{d} - 20\left(\frac{p}{d}\right)^{-13} + \frac{3.67}{90\left(\frac{p}{d}\right)^{2}}Pe^{\left(0.56+0.19\frac{p}{d}\right)}$$

which provides a similar gradient of *Nu* versus *Pe* in comparison with Westinghouse correlation in CIRCE-HERO operational conditions. For this reason, a constant multiplicative factor of 1.3, evaluated as the ration between Ushakov and Westinghouse correlations, is applied to the HTC.

RELAP5, developed and validated for water applications, does not consider heat conduction within the working fluid. This assumption could lead to no negligible errors in liquid metal systems. The influence of heat conduction on radial and axial directions in liquid metal natural circulation was investigated by Yoo et al. (2003). As presented in Narcisi et al. (2019a), axial conduction has no appreciable effect on the temperature distribution within an LBE fuel bundle, whereas radial conduction, whose effect is negligible for high liquid metal flow rate, assumes relevant importance when the mass flow decreases to values typical of natural circulation. At this purpose, 3456 heat transfer nodes are considered to reproduce the radial conduction between adjacent subchannels, considering the volume between the center of subchannels and assuming a “fake” material with negligible heat capacity and LBE thermal conductivity. A high HTC multiplicative factor is considered in order to exclude the convective resistance.

The rods cold tails pass through the test section up to the cover head of the fitting volume. Thermal inertia of the cold pins is considered with 3600 passive heat transfer nodes. In addition, 1728 passive nodes reproduce the heat losses between edge and corner subchannels and the cold pool; these heat structures include the hexagonal and cylindrical FPS casing and the stagnant LBE between the two layers.

A vertical pipe connects FPS model with fitting volume, which is simulated with a horizontal pipe component with variable flow area, to reproduce the flow path of the test section. Previous simulation activities (Narcisi et al., 2017a and Narcisi et al., 2019a) assess the importance of a detailed nodalization for this component, that gives rise to high heat losses towards the pool. The fitting volume is connected with the riser, modelled with a vertical pipe composed of 26 control volumes. At the riser inlet, a time dependent junction set the Ar injection flow rate. Inlet conditions of the gas are imposed with a time dependent volume. On the top, the separator operates as a hot pool. This component is modelled with two parallel pipes in order to reproduce the buoyancy within the large volume. A coarse axial meshing is adopted to limit the passage of the free level between two contiguous control volumes, that could cause instabilities on the LBE mass flow calculation, due to the large difference in density between liquid metal and cover gas. The separator is connected with the gas plenum, where the cover pressure is imposed with a time dependent volume, and with the steam generator.

The SG primary side is modelled with a single equivalent pipe component, reproducing the descending flow path of the LBE. 8680 heat transfer nodes are considered for the heat transfer between primary side and water/steam DWBTs annular riser. In order to obtain a better evaluation of the HTC on the primary side, according with Ushakov correlation (the most appropriate even in this case), a constant multiplicative factor of 1.02 is applied to the Westinghouse correlation. As mentioned above, a more detailed nodalization scheme of the secondary loop is developed for post-test calculations. The model includes the feeding pipe downstream the pre-heater, the manifold, seven DWBTs separately simulated, the steam chamber and the steam line up to the valve V3. For the secondary system, heat losses toward the environment are not considered. Each DWBT model includes two vertical channels, reproducing the feed water descending side and the annular riser (simulated with the annulus component). Seven heat structures simulate the heat exchanged between descending and ascending secondary side. Two time dependent volumes are considered, imposing feed-water inlet conditions downstream the pre-heater and secondary system pressure at the steam line outlet. The total feedwater mass flow rate is imposed with a time dependent junction. A K-loss coefficient is considered at the inlet of each DWBT, to consider local pressure drop induced by the turbine flow meter. The operation of secondary system is affected by uncertainties, mainly due to the lack of some parameters that make it difficult to understand the experimental operation. In the following, parameters acquired, and quantities not recorded by the monitoring system are summarized:

- Tube 0: FW flow rate is acquired over the whole test; the water/steam temperature is measured in 4 sections along the annular riser;
- Tube 1: FW flow rate is not acquired. During the full power operation, at the outlet section of the annular riser, the TC measured saturated temperature but no information about the static quality is available. The saturated conditions are reached due to the absence of the turbine FM, which reduces the pressure drops and, therefore, increases FW flow rate in this tube;
- Tube 2: FW flow rate and steam outlet temperature are not acquired;
- Tube 3: FW flow rate is acquired up to the transition event and steam outlet temperature is collected over the whole test;
- Tube 4: FW flow rate and steam outlet temperature are acquired over the whole test;
- Tube 5: FW flow rate is measured up to the transition event and steam outlet temperature is not acquired;

- Tube 6: FW flow rate and steam outlet temperature are not collected.

For these reasons, K-loss coefficients at the DWBTs inlets are calibrated in order to obtain correct steam temperature at the outlet of the bayonet element 0, 1, 3 and 4, during the full power operation. Given that turbine flow meters inserted in the tubes number 0 and 5 measure the same flow rate, the same K-loss coefficients are considered for these tubes. The rest of the feedwater mass flow rate is divided equally between tubes 2 and 6, for which no information is available. These assumptions are affected by the uncertainty related to the flow rate along tube 0, in which saturated conditions are obtained at the outlet section but information about steam quality is not available. In addition, a blockage is supposed to occur within the bayonet element number 6, trying to explain the superheated condition acquired at the inlet of this tube. To reproduce the blockage occurring after the transition event, a trip valve component is included within the DWBT number 6. The position of the valve was the subject of a sensitivity analysis. Four positions were considered:

- at the DWBT inlet section;
- into the annular riser, 650 mm above the bottom edge;
- into the annular riser, 2925 mm above the bottom edge;
- into the annular riser, 5325 mm above the bottom edge.

The blockage supposed close to the turbine flow meter did not allow the feeding of the bayonet element, causing boiling of the whole liquid phase contained within the DWBT 6. At the inlet section, temperature increase was overestimated of about 30 K. When the blockage was supposed to occur within the annular riser, steam came back up to the inlet section, where saturated conditions were obtained; superheated steam condition was not reached. The other three cases showed the same results, proving that inlet temperature did not depend on the position of the blockage within the annular riser. For the post-test simulation, the blockage is supposed to occur 5325 mm above the bottom edge of the bayonet element.

Figure 6 shows the MULTID component, developed for simulation of the cold pool. The three-dimensional model consists of 51 axial levels (z- coordinate), 4 radial meshes (r- coordinate) and 8 azimuthal intervals (theta-coordinate). The nodalization scheme on r- and theta- coordinates depends on the asymmetry of the test section, as presented in Figure 6, where the most representative sections are shown with the volumes occupied by internal components (these volumes are excluded from the computational array using calibrated porosity factors), and on the positions of the TCs support rods. On the z- coordinate, a detailed meshing is developed, following the axial nodalization of the primary flow path, according with the sliced modelling approach. It allows comparison of the calculated LBE temperature with the experimental acquisitions. Because LBE is free to move inside the pool, a high equivalent diameter is introduced in the MULTID component, limiting the wall friction.

The heat losses between primary flow path and cold pool are considered; several heat structures between each control volume of the TS model and the correct control volume of the MULTID component are introduced. In addition, heat losses towards the external environment are considered, assuming the outside temperature of 293 K and a constant HTC on the external surface of the vessel insulation. Within the main vessel, the HTC for non-bundle geometries is evaluated with Seban-Shimazaki correlation (The RELAP5-3D© Code Development Team, 2015b):

$$Nu = 5.0 + 0.025Pe^{0.8}$$

The main dimensions of the thermal-hydraulic model are summarized in Table 1.

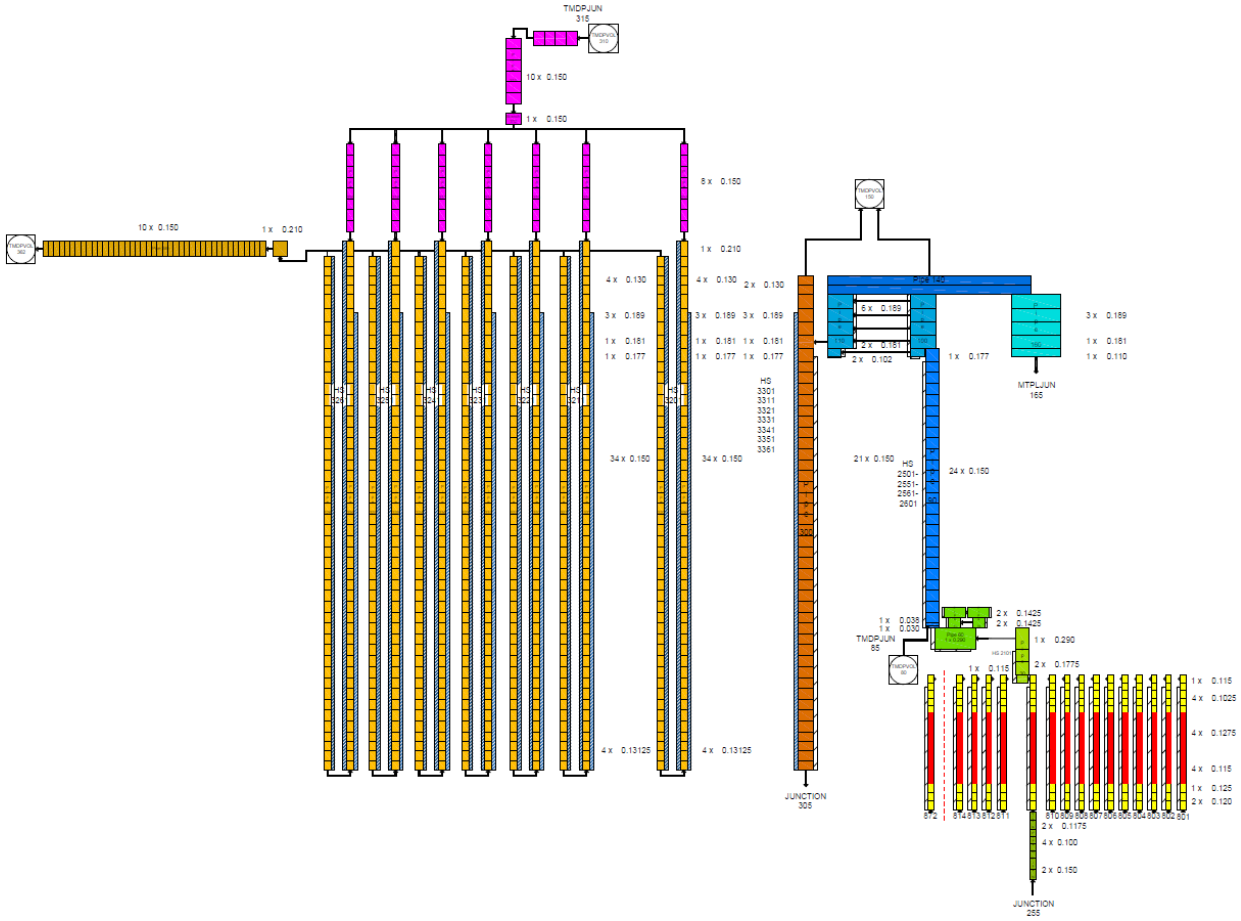

Figure 4. CIRCE-HERO mono-dimensional model

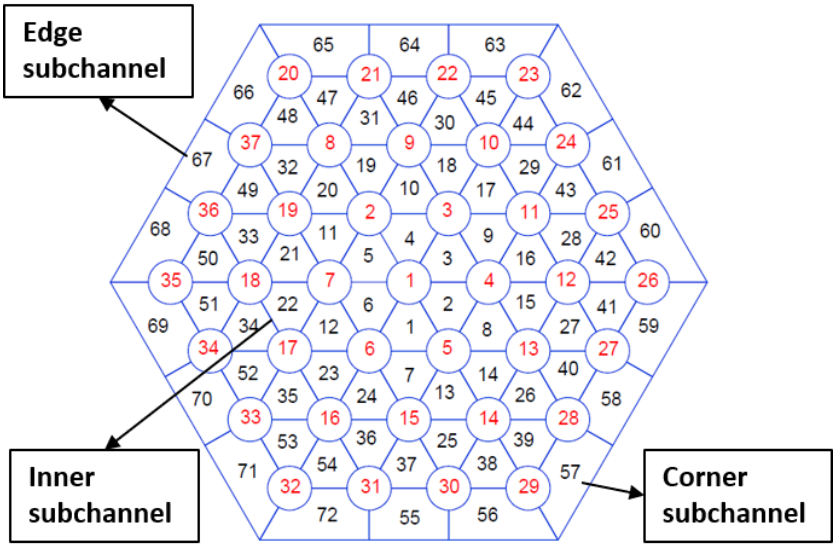

Figure 5. FPS subchannel modelling approach

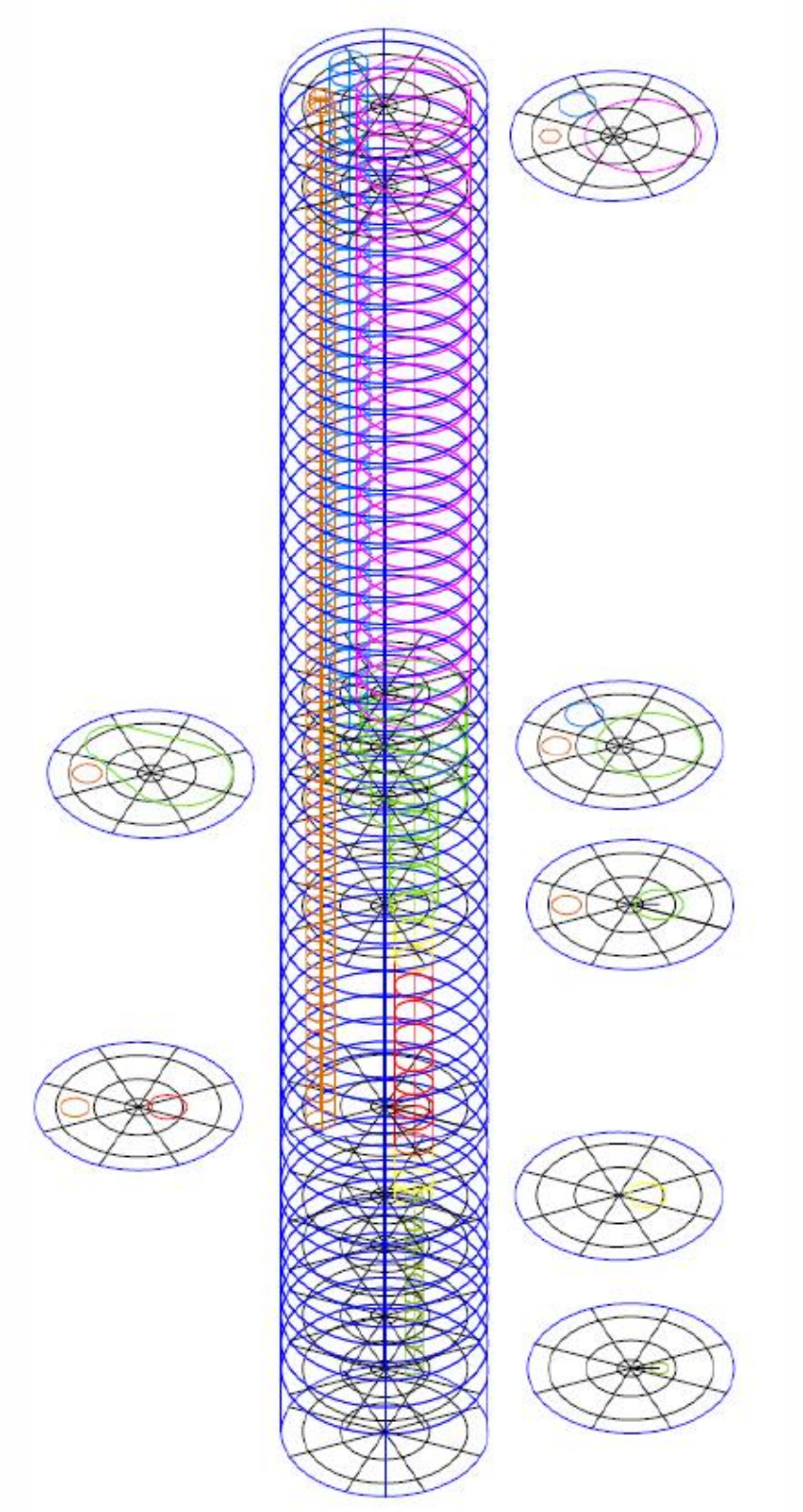

Figure 6. CIRCE-HERO multi-dimensional model

Table 1. Model dimensions

Parameter	Number of components
Hydrodynamic volumes	3599
Hydrodynamic junctions	8134
Heat structure mesh points	37953

4. Simulation activity

Calculations have been carried out with RELAP5-3D© ver. 4.3.4, adopting the most recent thermophysical LBE properties correlations, recommended by NEA (OECD/NEA Nuclear Committee, 2015) and integrated in R5-3D, as presented in Balestra et al. (2016). In the MULTID component, the three-dimensional momentum equations are used.

Initial conditions for the transient simulation have been obtained with a full power calculation, assuming the boundary conditions presented in section 2.2. Table 2 summarizes the simulation results, comparing them with experimental data. Discrepancies between simulation and experiment are compared with the measurement uncertainties and they are highlighted in green when the discrepancy is contained within uncertainty bands, and in red in the other case.

The experimental acquisition of LBE mass flow rate is affected by large uncertainties. The calibration and the accuracy estimation of the Venturi flow meter are described in Ambrosini et al. (2004) and Agostini et al. (2005), highlighting a relative error of about 25 % when mass flow assumes values lower than 50 kg/s. R5-3D calculates a primary flow rate of 31.4 kg/s, underestimating the average value acquired by the FM, even if the discrepancy is included within the uncertainty band. The good evaluation of the code is confirmed by the mass flow rate obtained by the energy balance (EB) equation, applied to the FPS, which provides LBE mass flow rate equal to 31.1 kg/s.

At the FPS inlet, the LBE temperature evaluated by R5-3D is compared with the average value of the temperature acquired by three thermocouples, highlighting a good agreement. Three TCs, placed at 120° from each other, measure LBE temperature at the FPS outlet holes. The average experimental data is compared with the mean temperature calculated by R5-3D at the highest control volume of channels 55, 61 and 67, showing a good agreement between experiment and calculation. Temperature drop between the FPS outlet and the SG inlet sections is due to the heat losses along the primary flow path. As shown in Table 2, the code well reproduces heat losses towards the pool, obtaining a good estimation of LBE temperature at the SG inlet holes. At the outlet section, experimental acquisitions show a large spread on the LBE temperature, highlighted by the large uncertainty reported in Table 2. The code shows an underestimation of LBE temperature drop across the SG, obtaining a large discrepancy with the experimental data.

On the secondary side, pressure losses through the DWBTs are calibrated in order to obtain a good estimation of the steam temperature at the outlet sections of tubes number 0, 1, 3 and 4. This assumption causes an overestimation of the flow rate through tubes 0, 3, 4 and 5. The discrepancies could be due to the lack of information presented in section 3.

Figure 7 shows the vertical trend of LBE temperature inside the pool during the full power steady state operation. The elevation is shown on the x axis, assuming the 0 level below the bottom plate of the separator and moving downward within the pool. The acquisitions of the TCs installed on rods A (Figure 7a) and H (Figure 7b) are compared with LBE temperature evaluated by R5-3D in the exact positions of the TCs (see Figure 3 for the location of the support rods). The analysis aims to assess the capability of MULTID component to reproduce three-dimensional thermal-hydraulic effects typical of large pool. Experiment shows that, at the same axial level, LBE assumes the same temperature in different azimuthal positions, whereas a relevant vertical stratification phenomenon occurs between -5 and -6 m, at the SG outlet level. The simulation is in good agreement with experimental data. The qualitative trend is well reproduced, predicting the relevant stratification phenomenon. In the upper part of the pool (between 0 and -5 m) an almost uniform profile is simulated, under predicting the experimental data of about 2 degrees. The magnitude of the stratification (about 50 K) is well reproduced and LBE temperature in the lower part of the pool (between -6 and -8 m) is in good agreement with experiment. Figure 8a provides a useful representation of LBE temperature within the test facility, observing the most relevant section that includes the FPS and the SG. The temperature within the pool is uniform from 0 to -5 m, assuming a value of about 745 K. This is due to the large amount of heat losses from the TS hottest part, in particular from the FPS and the fitting volume which are not insulated (the FPS is insulted with a double wall shell filled with stagnant LBE). Between -5 and -6 m, cold LBE, exiting the SG, cools the lower pool, causing the vertical stratification. Figure 8b shows the error distribution in the same axial section. Being the LBE temperature uniform at the same vertical levels, the TCs on rod A is considered for the comparison. In order to cover the whole pool along z- coordinate, the experimental temperatures are interpolated between two contiguous acquisition points, following the black line presented in Figure 7a. The representation shows the good agreement between the simulation and the experiment, except from -5.5 to -6.1 m, where discrepancy increases to 40 degrees, explained by the prediction of the stratification level about 0.25 m above the experimental data.

Table 2. Full power calculation: main results

Parameter	Unit	Experiment	Uncertainty	R5-3D	Error
LBE MFR	kg/s	34	25%	31.4	-7.6%
Av. FPS inlet T	K	692.8	2.0	693.6	0.8
Av. FPS outlet T	K	769.8	2.0	769.5	-0.3
Av- SG inlet T	K	759.9	2.0	761.3	1.4
Av. SG outlet T	K	674.1	12.0	687.1	13.0
TFM-T0	kg/s	0.0372	0.0044	0.0430	0.0058
TFM-T3	kg/s	0.0408	0.0044	0.0479	0.0071
TFM-T4	kg/s	0.0394	0.0044	0.0480	0.0086
TFM-T5	kg/s	0.0372	0.0044	0.0430	0.0058
TC-C0-O70	K	647.0	2.0	644.4	-2.6
TC-C1-O70	K	625.9	2.0	626.3	0.4
TC-C3-O70	K	633.9	2.0	633.9	0.0
TC-C4-O70	K	633.5	2.0	633.9	0.4

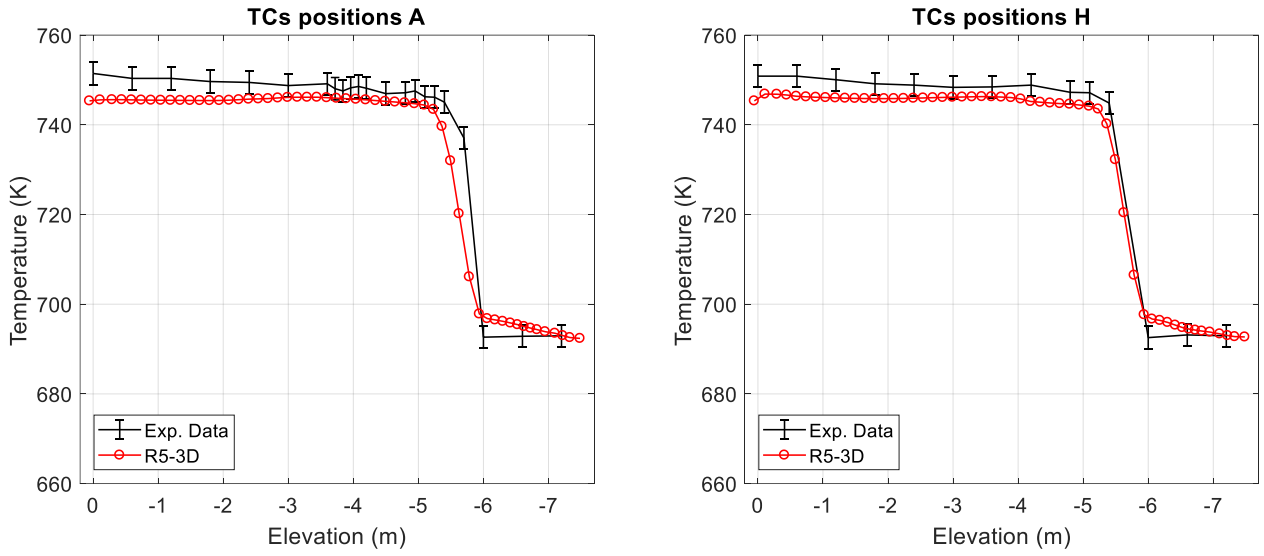

Figure 7. Pool thermal stratification: full power steady state conditions

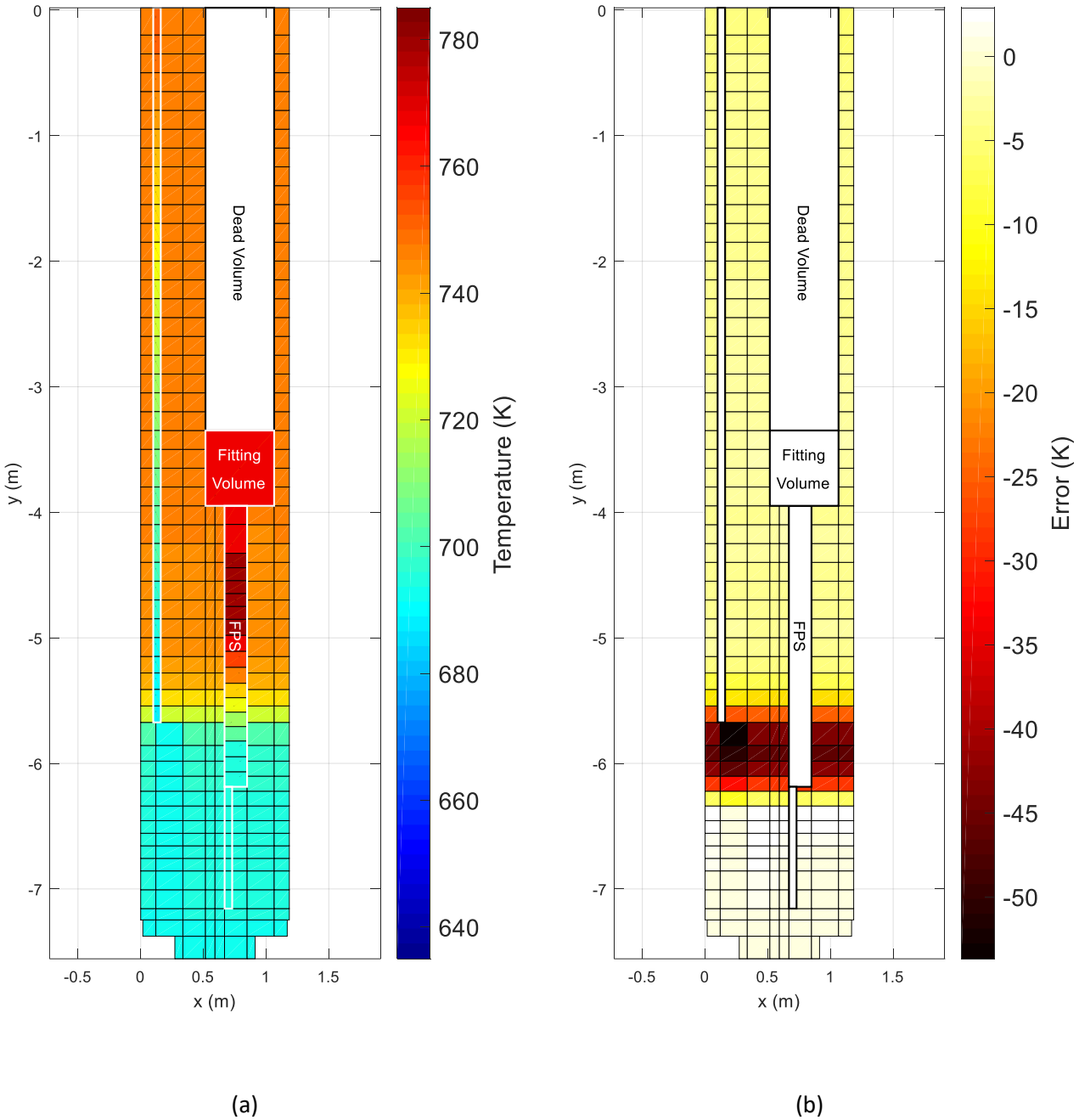

Figure 8. Pool temperature

Starting from the full power steady state conditions, transient analysis has been carried out. The boundary conditions are summarized in section 2.2. In the following plots, experimental data are compared with two calculations: case 1 (#1) assumes a total FW mass flow rate equal to 0.078 kg/s (reference value provided in Lorusso et al., 2019a) and case 2 (#2) adopts the value of 0.047 kg/s. The blind simulation highlighted an overestimation of the power remove by the SG (Lorusso et al., 2019b). In case 2, the feedwater mass flow rate has been calibrated in order to obtain the correct thermal power removed by the secondary system.

Acceptability of this assumption will be analyzed in the following. In the plots, experimental trends are presented with the mean value acquired by the instrumentations (solid line) and their uncertainty bands (dotted line).

Figure 9 compares the LBE mass flow rate acquired by the Venturi FM with the EB flow rate and the primary flow obtained by simulations. The quick decrease occurring after the transition event is well reproduced by the code and the two calculations do not show visible differences. When argon injection is cut off, the experimental monitoring system acquired the minimum value of primary flow rate (about 3 kg/s), well predicted by case 1 and under predicted by case 2 of about 2 kg/s. As discussed in section 3, the improved thermal hydraulic model provides a better estimation of the flow rate, avoiding the establishment of the reverse flow condition, observed in the blind simulations. After that, the simulated flow rate increases slower than experimental data up to the new quasi steady state condition. The natural circulation depends on the heat source (FPS power), the heat sink (power removed by SG) and the relative distance between them. The difference of secondary flow rate produces a discrepancy in terms of primary flow of about 1 kg/s between the two calculations. Both the results are included within the uncertainty band but case 2 provides the best estimation of the experimental acquisition. The EB value is outside the experimental uncertainty band but, in natural circulation, it is expected that the uncertainty increases over the reference value of 25%.

Figure 10 shows the temperature increase through the HS active length, comparing temperature acquired by thermocouples T-FPS-31, 35 and 36 with simulations results obtained in the exact position of instrumentation (respectively at the inlet and outlet section of the subchannel 01 and at the outlet section of the subchannel 29). At the top of the active length, the rapid temperature decrease is well predicted by the calculations, not presenting visible differences. When the FPS power reaches the decay heat value, LBE mass flow rate still assumes 50 % of the nominal value, causing the minimum temperature at the outlet of the HS active length. This effect is well predicted by both the simulations, reaching a minimum value of about 710 K. When the Ar injection system is cut off, and the LBE MFR assumes the minimum value, at the outlet section of the HS active length the LBE temperature rapidly increases up to the maximum value of 740 K, acquired by the TC T-FPS-35 at 155 s. Calculation #1 matches very well the experimental trend, assuming the same maximum temperature. At this time, the LBE mass flow calculated by R5-3D approaches the EB trend, proving that this value must be considered as the reference primary flow rate. Simulation #2 well reproduces the first seconds of the temperature ramp, but the maximum value is overestimated (about 8 degrees) and delayed (about 25 s) than the experimental data. This is explained by the under prediction of the primary flow rate up to 250 s. In the long term, case 1 predicts too high temperature gradient, leading to underestimation of the inlet temperature at FPS inlet (more than 2 degrees at the end of the test). At the outlet section, the over prediction of LBE mass flow causes a lower value of the temperature increase than the experiment and an underestimation of the outlet temperature of about 12 K at the end of the test. The lower secondary flow rate assumed in the second calculation, provides a better estimation of the temperature gradient (the inlet temperature approaches very well the experimental data) and the good agreement in terms of primary mass flow rate ensures a good prediction of the outlet temperature.

Figure 11 shows the temperature decrease through the SG primary side. Experimental temperatures are acquired at the SG inlet holes, at 4200, 3000 and 1500 mm from the bottom of the heat exchanger and at the SG outlet. At the top of the test section, the separator operates as a hot pool; the large amount of hot LBE reduces the cooling trend observed at the FPS outlet. This effect is well reproduced by simulations, even if R5-3D under predicts the inlet temperature after the transition. This is due to the SG modelling approach, collapsing the LBE subchannel in a single equivalent pipe. At the top of the SG, TCs are installed at the inlet holes and the higher temperature acquired by instrumentation than the computed values is explained by the boundary effects. Looking at the outlet section, both the calculations predict a peak temperature at about 95 s from the beginning of the test. This is due to the rapid decrease of the FW flow rate in the face of a slower primary flow reduction.

This behavior is not observed by experimental acquisitions. Along the SG, feedwater mass flow rate of 0.047 kg/s allows a better estimation of the whole temperature drop and of the heat exchanger efficiency in the different axial sectors. In case 1, the higher amount of temperature drop occurs in the upper part of the SG, from 3000 mm to the inlet holes. Instead, case 2 allows a better partition of the total temperature drop along the SG, matching very well experimental data in each monitored section. This is due to a better evaluation of the power removed by the SG and of the primary mass flow rate. The thermal power removed is shown in Figure 12, where experimental data is obtained with the energy balance equation applied to the SG primary side. Figure 12 shows that case 1 over predicts the power removed over the whole transient test (even if it is included within the uncertainty bands), whereas the secondary flow rate imposed to the calculation #2 has been calibrated to obtain the correct SG power.

Figure 13 shows thermal stratification at the end of transient test, comparing experimental data acquired on the support rods A and H with computational results. Due to unbalance conditions occurring after the transition from GEC to NC, the TCs observe a reduction of the average pool temperature (about 10 degrees), even if the qualitative vertical trend is maintained (thermal stratification is still observed between -5 and -6 m). R5-3D is able to reproduce the progressive pool cooling, matching very well LBE temperature in the upper part in both the calculations (740 K). At the bottom, the under prediction of SG outlet temperature leads to underestimation of LBE temperature within the pool by calculation #1 whereas case 2 is in good agreement with experiment.

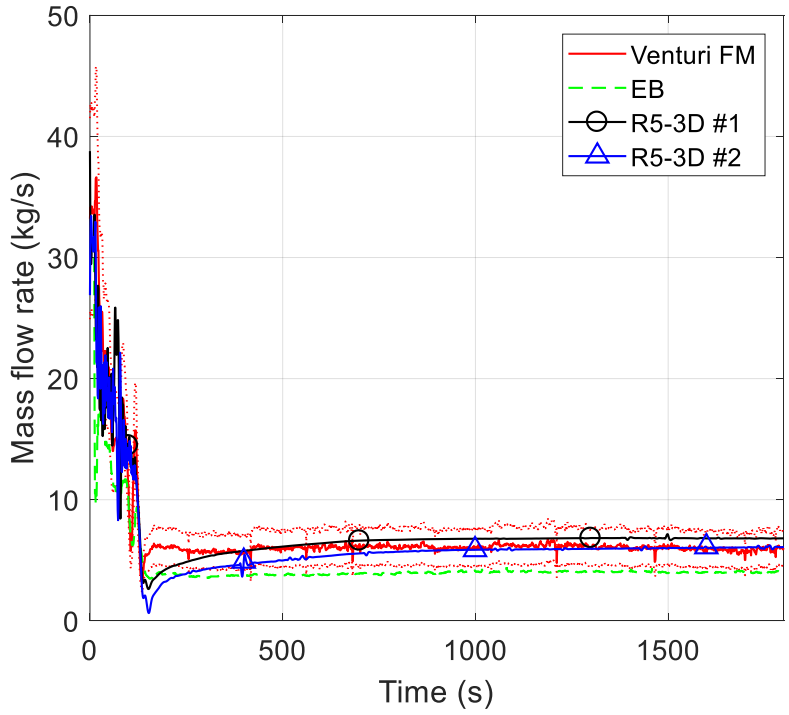

Figure 9. LBE mass flow rate

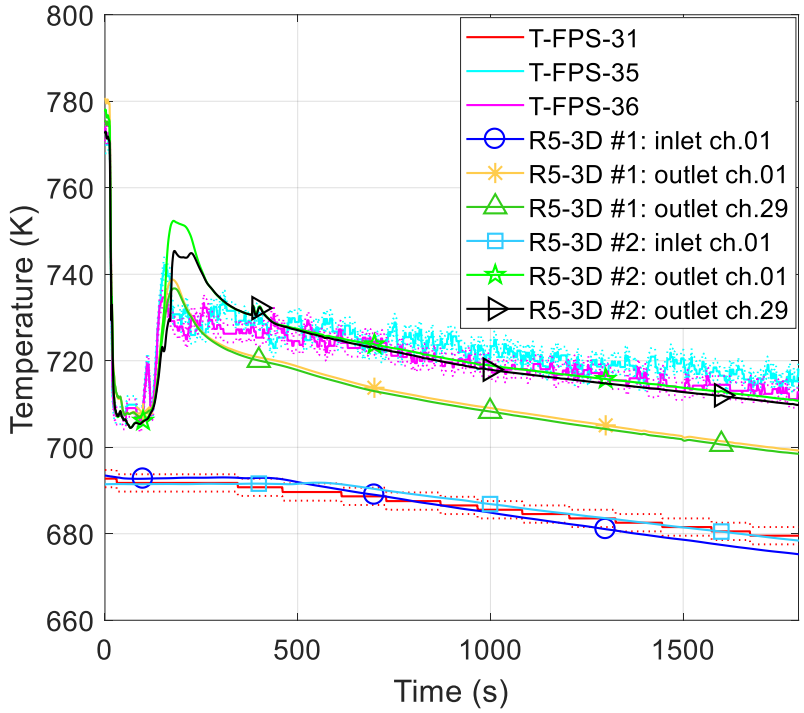

Figure 10. FPS inlet and outlet temperature

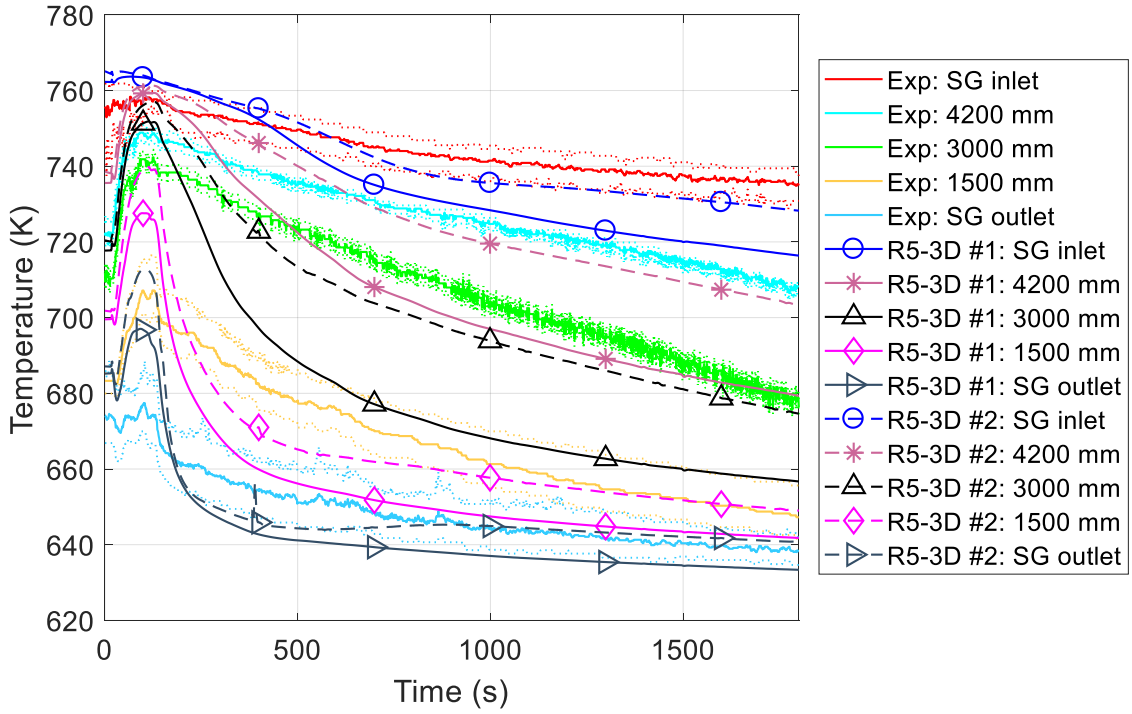

Figure 11. LBE temperature through the SG

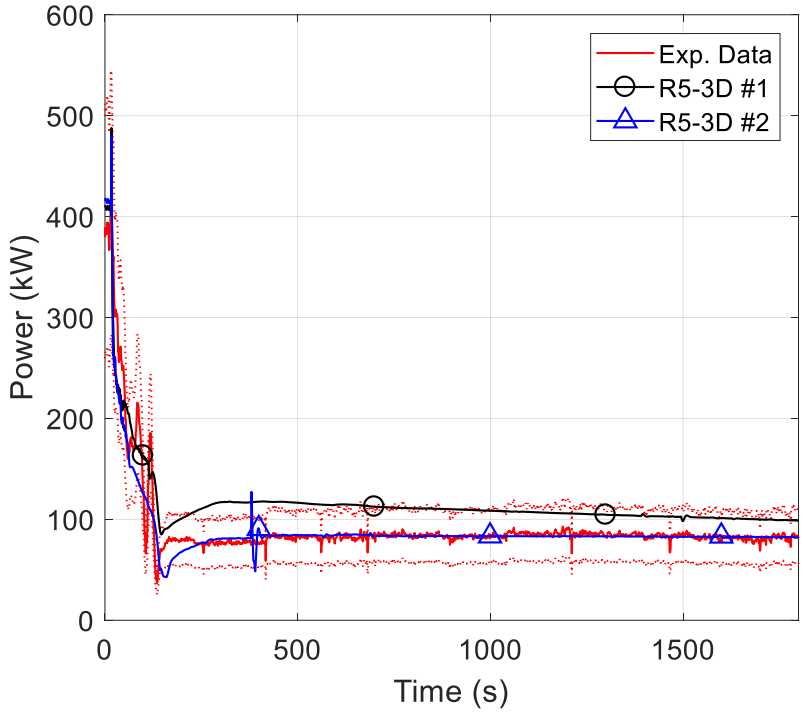

Figure 12. Power removed by the SG

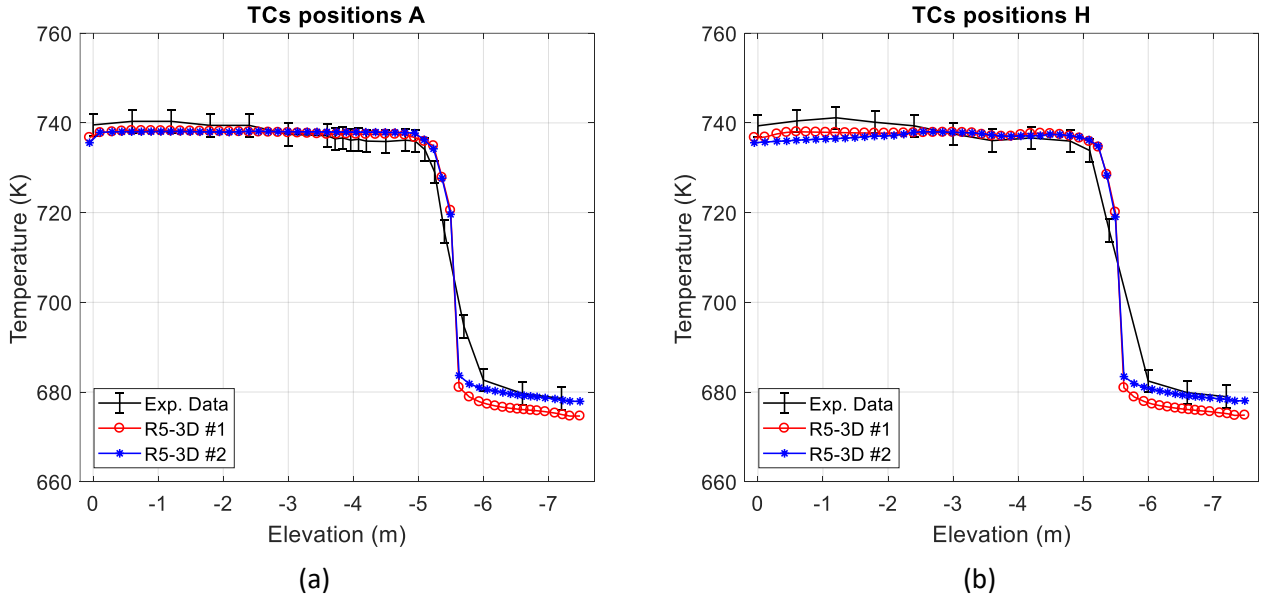

Figure 13. Pool thermal stratification: final conditions

Regarding the secondary loop operation, Figure 14 compares mass flow rate measured by turbine flow meters at the inlet sections of DWBTs 0 (a) and 4 (b) with simulations results. The others flow meters lost the signal after the transition event. For case 1, the total FW mass flow rate is assumed equal to the reference data of 0.078 kg/s (Lorusso et al., 2019a); Figure 14 shows that, in this case, R5-3D results are in good agreement with the best

estimation of the experimental measurements. Reducing the total flow rate to 0.047 kg/s, the experimental acquisitions are under predicted, even if computational results remain within the uncertainty bands. Figure 15 shows steam temperature at the outlet of tubes 0, 1, 3 and 4, comparing experimental data with simulation results. After the transition, R5-3D over predicts the sharp temperature increase, overestimating the maximum temperature of about 35 degrees in both the simulations. At the DWBTs outlet, steam assumes temperature only few degrees lower than LBE temperature on the primary side. It could be due to the thermal conductivity of the powder within the DWBT, which could be overestimated in the modelling. After that, calculation #1 over predicts steam temperature gradient, observing a faster decrease than the experiment. Despite this, reducing the secondary flow rate, the gradient calculated by R5-3D is in good agreement with the experimental trend, even if steam temperature remains higher than the TCs acquisition over the whole test.

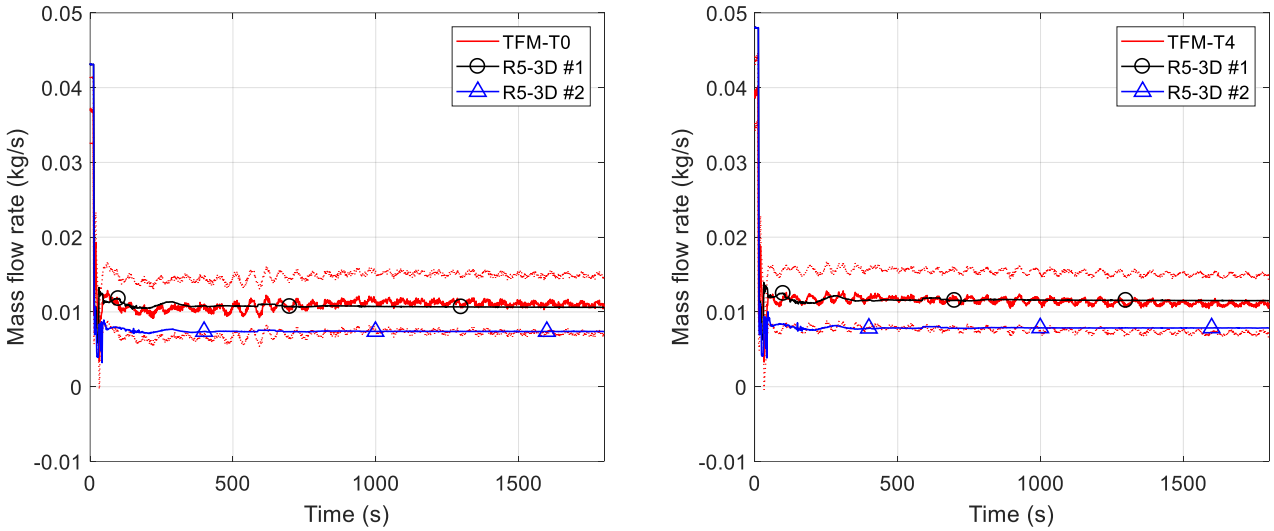

Figure 14. FW mass flow rate through DWBTs 0 and 4

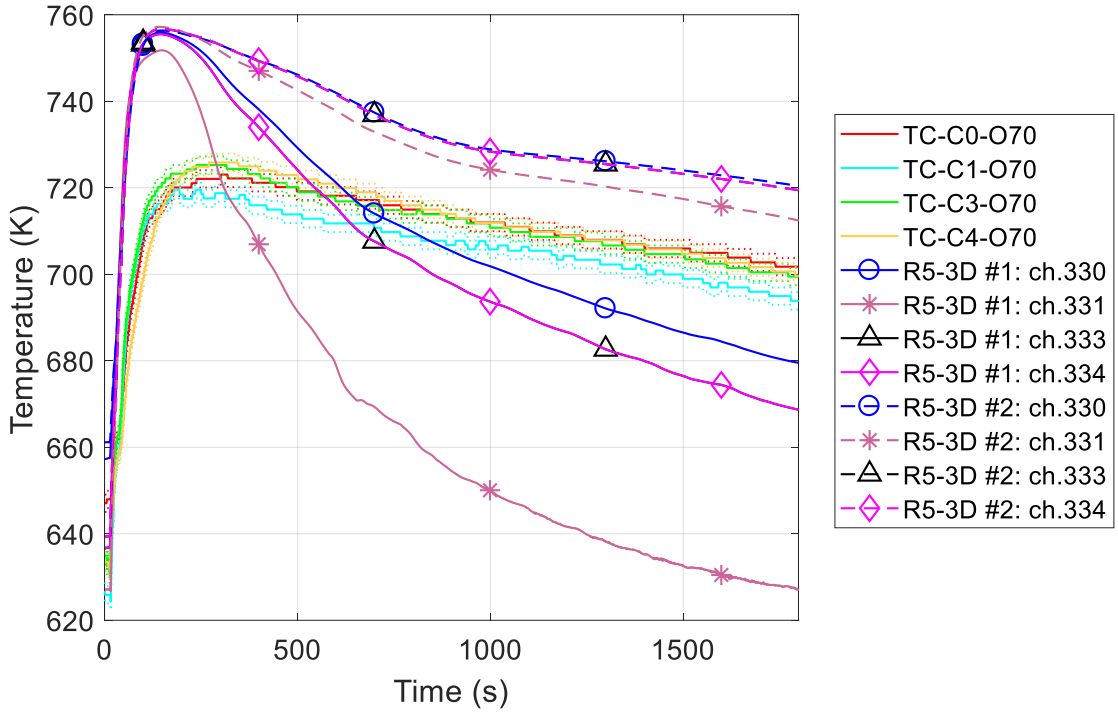

Figure 15. Steam outlet temperature

5. Conclusions

The experimental test performed on CIRCE-HERO test facility offered useful data for validation of computational codes, improved with capabilities to simulate innovative HLM nuclear systems. CIRCE-HERO facility was designed to reproduce an HLM-cooled pool-type reactor, testing a DWBT SG in a relevant configuration for ALFRED SG. The experimental campaign concerned a protected loss of flow accident, reproducing the primary pump cut off simulating the presence of a pump flywheel, the consequent reactor scram and the activation of the DHR system.

The experimental campaign was proposed for a validation benchmark in the framework of the H2020 SESAME project. “Sapienza” University of Rome performed the pre-test analysis, developing the CIRCE-HERO thermal-hydraulic model starting from the validated CIRCE-ICE nodalization scheme. The model, developed with RELAP5-3D©, was focused on the analysis of primary flow path and LBE pool thermal-hydraulics, providing useful information to the experimentalists.

As a participant of the benchmark exercise, “Sapienza” used CIRCE-HERO model to carry out blind-calculations. The open phase of test benchmark highlighted the over prediction of the SG performances obtained with the blind simulation. The analysis of experimental campaign suggested a revision of the thermal-hydraulic model, improving the nodalization scheme of secondary loop to consider the asymmetries in the parallel tubes.

The thermal hydraulic model consists of mono-dimensional scheme of the primary flow path and the secondary loop, and multi-dimensional nodalization of the LBE pool. A detailed meshing of the main components is developed: the FPS is analyzed subchannel per subchannel, with 72 parallel pipes with cross junctions, and the seven double wall bayonet tubes are separately modelled.

The simulation activity presented in this paper is aimed on the assessment RELAP5-3D capabilities to reproduce the main thermal-hydraulic features of an HLM-cooled pool-type reactor, in safety relevant operation conditions. Assuming boundary conditions provided by ENEA, full power calculations have been carried out. The simulation results are globally in agreement with experimental data for all the primary circuit physical quantities monitored; some discrepancies are highlighted on the secondary side, where total mass flow rate is assumed equal to the best estimate measurement of the Coriolis flow meter and pressure losses at the inlet of the bayonet elements are calibrated to obtain the correct steam temperature at each outlet. An overestimation of about 15% is observed on the flow rate through the DWBTs 0, 3, 4 and 5. Discrepancies are explained by the lack of some information which determines large uncertainties on the evaluation of secondary system boundary conditions. One of the main tasks of the simulation activity has been the assessment of MULTID capability to reproduce relevant thermal-hydraulic phenomena within a large pool. At this purpose, 119 TCs installed within CIRCE pool provide useful data for code validation. Comparison with experimental data highlights excellent capabilities of the multi-dimensional component to reproduce the heat losses between hot leg and LBE pool. The code is able to reproduce steady state vertical profile of the temperature, matching very well the experimental thermal stratification occurring at the SG outlet level. In addition, MULTID component well reproduces the pool temperature trend over the whole transient test.

Starting from the full power steady state conditions, two transient calculations have been performed, assuming the same boundary conditions, except for the total feedwater mass flow rate after the transition event. Case 1 assumes the reference value of the secondary flow rate (0.078 kg/s), obtained with the energy balance equation applied to the FW pre-heater. This calculation highlights an overestimation of the power removed by the SG; for this reason, a second calculation has been performed calibrating the total secondary flow rate to 0.047 kg/s which guarantees the correct SG power. Both the simulations are in good agreement with experimental data in the first 200 s, reproducing very well the first minutes after the transition event. After the Ar injection cut off, the first calculation provides a good estimation of the minimum value of the LBE MFR, underpredicted by the second calculation of about 2 kg/s. The long-term behavior strongly depends on the feedwater mass flow rate. Case 1 shows an overestimation of the whole system energy unbalance, leading to the over prediction of the natural circulation contribution and of the cooling trend. The SG power balance analysis highlighted an overestimation of the power removed of about 30% of the experimental value. The large uncertainties related to the measurement of the secondary system quantities have suggested the calibration of the secondary flow rate to obtain the correct SG power removed. This assumption has been justified comparing the experimental flow rate, acquired at the inlet of the tubes 0 and 4, with the simulation results: the experimental data are underestimated but the calculation results remain within the experimental uncertainty bands. Looking at the primary system, the assumption of a lower FW flow rate leads to a better agreement with experimental data, providing a good estimation of the long-term behavior. Some discrepancies are still maintained on the secondary side, where the steam outlet temperature is over predicted by the code. The differences could be due to a not perfect agreement of the powder thermal conductivity, which represents a large source of uncertainties. This opens the possibility to continue the post-test analysis for the secondary side, leading an improved experimental results analysis, despite of the good global results obtained.

Acknowledgment

This work was performed in the framework of H2020 SESAME project. This project has received funding from Euratom research and training program 2014-2018 under grant agreement No 654935.

Nomenclature

CIRCE	CIRColazione Eutettico
DHR	Decay Heat Removal system
FM	Flow Meter
FPS	Fuel Pin Simulator
FW	Feed-Water
GEC	Gas-Enhanced Circulation
HERO	Heavy liquid mEtal pRessurized water cOoled tubes
HLM	Heavy Liquid Metal
HTC	Heat Transfer Coefficient
LWR	Light-Water cooled Reactor
MFR	Mass Flow Rate
MULTID	Multi-dimensional
NC	Natural Circulation
PLOFA	Protected Loss Of Flow Accident
R5-3D	RELAP5-3D
TB	Thermal Balance
TC	Thermocouple
TH-SYS	Thermal-Hydraulic System code
TS	Test Section

References

Agostini, P., Alemberti, A., Ambrosini, W., Benamati, G., Bertacci, G., Cinotti, L., Elmi, N., Forgione, N., Oriolo, F., Scadozzo, G., Tarantino, M., 2005. Testing and qualification of CIRCE Venturi-nozzle flow meter for large scale experiments. Proc. 13th Int. Conf. Nucl. Eng., Beijing, China. DOI: 10.1115/ICONE13-50909

Ambrosini, W., Azzati, M., Benamati, G., Bertacci, G., Cinotti, L., Forgione, N., Oriolo, F., Scadozzo, G., Tarantino, M., 2004. Testing and qualification of CIRCE instrumentation based on bubble tubes. Jou. Nuc. Mat. 335, 293-298. DOI: 10.1016/j.jnucmat.2004.07.030

Angelucci, M., Martelli, D., Barone, G., Di Piazza, I., Forgione, N., 2017. STH-CFD Codes Coupled Calculations Applied to HLM Loop and Pool Systems. Sci. Tech. Nucl. Ins., Vol. 2017, DOI: 10.1155/2017/1936894

Balestra P., Giannetti F., Caruso G., Alfonsi A., 2016. New RELAP5-3D lead and LBE thermophysical properties implementation for safety analysis of Gen IV reactors. Sci. Technol. Nucl. Install., vol. 2016. http://dx.doi.org/10.1155/2016/1687946.

Bandini, G., Polidori, M., Meloni, P., Tarantino, M., Di Piazza, I., 2015. RELAP5 and SIMMER-III code assessment on CIRCE decay heat removal experiments. Nucl. Eng. Des. 281, 39-50. http://dx.doi.org/10.10167j.nucengdes.2014.11.005

Edemetti F., Tassone A., Narcisi V., Giannetti F., Ferroni L., Tarantino M., 2019. Numerical analysis of temperature stratification in the CIRCE pool facility. J. Phys. Conf. Ser. 1224 (012007). doi:10.1088/1742-6596/1224/1/012007

Frignani M., Grasso G., Tarantino M., Constantin M., Turcu I., Di Gabriele F., Romanello V., Alemberti A., 2017. FALCON advancedments towards the implementation of the ALFRED Project. Proc. Int. Con. Fast Reac. Rel. Fuel Cycl.: Next Gen. Nucl. Syst. Sust. Dev. Yekaterinburg, Russian Federation.

Giannetti, F., Di Maio, D.V., Naviglio, A., Caruso, G., 2016. Thermal-hydraulic analysis of an innovative decay heat removal system for lead-cooled fast reactors. Nucl. Eng. Des. 305, 168-178. http://dx.doi.org/10.1016/j.nucengdes.2016.05.005

Idelchik, I.E., 1986. Handbook of Hydraulic Resistance. Second ed. Hemisphere Publishing Corporation.

Lorusso P., Pesetti A., Tarantino M., 2018. ALFRED Steam Generator Assessment: design and pre-test analysis of HERO experiment, Proceedings of the 2018 26th International Conference on Nuclear Engineering, July 22-26, 2018, London, England, ICONE26-81824, DOI: 10.1115/ICONE26-81824.

Lorusso P., Pesetti A., Tarantino M., Narcisi V., Giannetti F., Forgione N., Del Nevo A., 2019a. Experimental analysis of stationary and transient scenarios of ALFRED steam generator bayonet tube in CIRCE-HERO facility. Nucl. Eng. Des., vol. 352, 110169, https://doi.org/10.1016/j.nucengdes.2019.110169

Lorusso P., Pesetti A., Tarantino M., Narcisi V., 2019b. Protected loss of flow accident simulation in CIRCE-HERO facility: experimental test and system code assessment, Proceedings of the 2019 27th International Conference on Nuclear Engineering, May 19-24, 2019, Ibaraki, Japan.

Memmott, M., Buongiorno, J., Hejzlar, P., 2010. On the use of RELAP5-3D as a subchannel analysis code. Nucl. Eng. Des. 240, 807-815. DOI: 10.1016/j.nucengdes.2009.11.006

Narcisi V., Giannetti F., Tarantino M., Martelli D., Caruso G., 2017a. Pool temperature stratification analysis in CIRCE-ICE facility with RELAP5-3D© model and comparison with experimental tests. J. Phys. Conf. Ser.,923 (012006). http://dx.doi.org/10.1088/1742-6596/923/1/012006.

Narcisi, V., Giannetti, F., Del Nevo, A., Tarantino, M., Caruso, G., 2017b. Pre-test analysis of protected loss of primary pump transients in CIRCE-HERO facility. J. Phys. Conf. Ser. 923 (012005). https://doi.org/10.1088/1742-6596/923/1/012005

Narcisi V., Giannetti F., Del Nevo A., Tarantino M., Caruso G., 2018. Pre-test analysis of accidental transients for ALFRED SGBT mock-up characterization. Nucl. Eng. Des., vol. 333, pp. 181-195, https://doi.org/10.1016/j.nucengdes.2018.04.015

Narcisi V., Giannetti F., Caruso G., 2019a. Investigation on RELAP5-3D© capability to predict thermal stratification in liquid metal pool-type system and comparison with experimental data. Nucl. Eng. Des., vol. 352, 110152, https://doi.org/10.1016/j.nucengdes.2019.110152

Narcisi V., Giannetti, F., Del Nevo A., Alcaro F., Wang X., Kraus A., Brunett A., Thomas J., Girault N., Grosjean B., Caruso G., Gerschenfeld A., 2019b. System thermal-hydraulic modelling of the Phénix dissymmetric test benchmark. Nucl. Eng. Des., in this issue.

OECD/NEA Nuclear Science Committee, 2015. Handbook on Lead-bismuth Eutectic Alloy and Lead Properties, Materials Compatibility, Thermal-hydraulics and Technologies.

OECD Nuclear Energy Agency – GIF, 2017. GIF Annual Report 2017. https://www.gen-4.org/gif/upload/docs/application/pdf/2018-09/gif_annual_report_2017_210918.pdf.

Schikorr, M., Bubelis, E., Mansani, L., Litfin, K., 2010. Proposal for pressure drop prediction for a fuel bundle with grid spacers using Rehme pressure drop correlations. Nucl. Eng. Des. 240, 1830-1842, DOI: 10.1016/j.nucengdes.2010.03.039, 2010

SESAME Project, EURATOM H2020, Grant Agreement N. 654935, April 2015.

Tarantino M., Martelli D., Barone G., Di Piazza I., Forgione N., 2015. Mixed convection and stratification phenomena in a heavy liquid metal pool. Nucl. Eng. Des., vol. 286, pp. 261-277. http://dx.doi.org/10.1016/j.nucengdes.2015.02.012

The RELAP5-3D© Code Development Team, 2015a. RELAP5-3D Code Manual Vol. I: Code Structure, System Models and Solution Methods. INL/MIS-15-36723, vol. 1, rev. 4.3.

The RELAP5-3D© Code Development Team, 2015b. RELAP5-3D Code Manual Vol. IV: Models and Correlations. INL/MIS-15-36723, vol. 4, rev. 4.3.

Turroni P., Cinotti L., Corsini G., Mansani L., 2001. The CIRCE test facility. ANS Winter Meeting AccApp. Reno, Nevada; USA.

Ushakov P.A., Zhukov A.V., Matyukhin N.M., 1977. Heat transfer to liquid metals in regular arrays of fuel elements. High Temp. vol. 15, pp. 868–873 translated from Teplofizika Vysokikh Temperatur, vol. 15 (1977), pp. 1027–1033

Yoo Y.J., Sabharwall P., Reyes J.N., Wu Q., Sienicki J.J., 2003. Effects of the fluid axial conduction on liquid metal natural circulation and linear stability. In: 2003 ANS/ENS International Winter Meeting, New Orleans, LA, pp. 1523-1530.

Zwijsen K., Dovizio D., Moreau V., Roelofs F., 2019. CFD modelling of the CIRCE facility. Nucl. Eng. Des., in this issue.